Applied Thermal Engineering 274 (2025) 126564

Contents lists available at ScienceDirect

Applied Thermal Engineering

journal homepage: www.elsevier.com/locate/ate

Research Paper

Heat transfer enhancement in shell and tube Latent Heat Thermal Energy Storage units for waste heat recovery applications: A 3D numerical study on melting–solidification kinetics

Soumaya Sokakini [a,*], Jules Voguelin Simo Tala [a], Lionel Nadau [b], Adrian Ilinca [c], Daniel Bougeard [a]

[a] IMT Nord Europe, Institut Mines-Télécom, Univ. Lille, Centre for Energy and Environment, F-59000 Lille, France
[b] ENGIE Lab CRIGEN, 4 rue Joséphine Baker, 93240 Stains, France
[c] Department of Mechanical Engineering, École de Technologie Supérieure, Montreal, QC H3C 1K3, Canada

ARTICLE INFO

Keywords:
Latent heat storage
Phase change material
Finned multi-tube
Heat transfer enhancement
Melting and solidification dynamics

ABSTRACT

This study presents a novel three-dimensional (3D) numerical investigation of a finned diamond-shaped multi-tube latent heat thermal energy storage (LHTES) unit for low-temperature industrial waste heat recovery applications. Unlike existing studies that rely on simplified two-dimensional (2D) simulations and square shaped tubes geometry, this work introduces an innovative diamond-shaped tube configuration with longitudinal fins, enhancing both melting and solidification dynamics. The proposed heat storage unit is compared at iso-volume of PCM to a finless multi-tube unit, considered a reference case. Using erythritol as phase change material (PCM) and Hytherm 600 as heat transfer fluid (HTF), the study demonstrates that the proposed design achieves reductions of 24.5 % and 45.5 % in the melting and solidification times, respectively, compared to a finless reference case. Additionally, the influence of axial temperature gradients and Reynolds number variations on phase change dynamics is thoroughly examined, revealing non-negligible three-dimensional effects and significant improvements in heat transfer performance. The axial temperature gradient in the tubes and the tridimensionality effect involved influence phase change dynamics with a difference exceeding 17 % and 16.36 % in melting and solidification, respectively. Moreover, the Reynolds number effect is more significant during the melting process and for the enhanced configuration. Up to 14 % and 8 % reductions in melting and solidification times is achieved for the improved configuration, compared with 12.1 % and only 3 % for the reference case when the Reynolds number was increased from 1000 to 2000.

1. Introduction

Since the Industrial Revolution, the greenhouse effect and carbon emissions have increased exponentially, resulting in a global environmental emergency. Concurrently, the globe is facing an unprecedented energy crisis driven by population growth, overproduction, consumption, etc. Given the gravity of the situation, it is critical to implement long-term and sustainable solutions to this problem. Waste heat recovery and valorization via heat storage constitute one of the most promising approaches to addressing both issues. By capturing and valorizing the massive amount of waste heat produced by industries, usually in the form of exhaust fumes, CO2 emission will be reduced. This waste heat can be reused for various applications such as heating, producing hot water, and supplying heat to other industrial endothermic processes, lowering energy requirements and reliance on fossil fuels. Until valorization, waste heat can be stored in sensible, latent, or thermochemical forms. Among these, latent heat storage is a good compromise solution, with greater maturity than thermochemical storage and higher energy density compared to sensible heat storage, enabling the storage of a large amount of energy in a relatively small volume [1]. However, a significant problem with this type of storage is the low conductivity of phase change materials (PCMs). This leads to limited heat exchange between the PCM and heat transfer fluid (HTF) and, thus, longer charging and discharging times. It is, therefore, problematic when used in processes that require faster charging and discharging times, such as off-site heat valorization. To tackle this problem, several studies with various enhancement techniques have been suggested, which can be classified into two categories: thermal conductivity and heat transfer enhancement. Thermal conductivity enhancement techniques include the addition of nanoparticles [2,3],

* Corresponding author.
E-mail address: soumaya.sokakini@imt-nord-europe.fr (S. Sokakini).

https://doi.org/10.1016/j.applthermaleng.2025.126564
Received 27 November 2024; Received in revised form 22 February 2025; Accepted 21 April 2025
Available online 5 May 2025

Nomenclature

Principle notations

C_p	Specific heat capacity (J kg^{-1} K^{-1})
D	Diameter (m)
f_l	Liquid volume fraction -
f_s	Solid volume fraction -
h	Sensible enthalpy per unit mass (J kg^{-1})
g	Gravity acceleration (m s^{-2})
H	Total enthalpy per unit mass (J kg^{-1})
L	Latent heat (J kg^{-1})
Re	Reynolds number -
t	Time (s)
T	Temperature (°C)
$\vec{V}$	Velocity vector (m s^{-1})
U	Velocity magnitude (m s^{-1})
P	Pressure (Pa)
Po	Heat duty (W)
x,y,z	Cartesian coordinates (m)

Greek symbols

β	Thermal expansion coefficient (K^{-1})
ϵ	numerical coefficient (–)
λ	Thermal conductivity (W m^{-1} K^{-1})
μ	Dynamic viscosity (Pa s)
ρ	Density (kg m^{-3})

Abbreviations

HTF	Heat Transfer Fluid
PCM	Phase Change Material
CFD	Computational Fluid Dynamics
LHTES	Latent Heat Thermal Energy Storage
MT-LHTES	Multi-Tube Latent Heat Thermal Energy Storage
FMT-LHTES	Finned Multi-Tube Latent Heat Thermal Energy Storage

Subscripts

ref	Reference
l	Liquidus
s	Solidus
0	Initial
full	Full phase change

expanded graphite [4], metal foam [5,6] and encapsulation [7], whilst heat transfer enhancement involve the use of multiple PCMs [8] or extended heat transfer surfaces such as fins and multiple tubes, etc.

Among the enhancement methods, adding fins to latent heat thermal energy storage (LHTES) units is considered one of the simplest and most cost-effective approaches [9]. That makes it more appealing to the scientific community, which has carried out numerous studies with a wide variety of fin designs, such as longitudinal, annular, helical, Y-shaped, and tree-shaped fins, etc [10–15]. These studies have demonstrated the effectiveness of fins installation in heat transfer enhancement. Yang et al. [10] conducted a 2D numerical study of a shell-and-tube system with and without annular fins. Their results showed that by using annular fins, melting time can be reduced by up to 65%. Kirincic et al. [11] presented a 3D numerical study investigating the influence of adding longitudinal fins to a vertically oriented shell-and-tube LHTES system. The total melting and solidification times were reduced by 52 and 43, respectively. Yuan et al. [12] evaluated the longitudinal fin arrangement effect by comparing five installation angles. The findings indicated that the vertical orientation at an angle of 0° has the quickest melting time and that increasing the fin's angle above 45 °C has no significant effect. Liu et al. [13] proposed a novel structure with ladder-shaped fins. Up to 52.2% in melting time was saved by using the ladder-shaped fins instead of straight fins. Yu et al. [14] carried out a 2D numerical analysis to examine the performance of Y-shaped fins in the solidification process. Compared to straight longitudinal fins, Y-shaped fins provided a more uniform temperature field and shortened solidification time by 50.9%. Furthermore, when optimizing design parameters, this reduction was improved to 71.5%. Mahdi et al. [15] compared the annular, longitudinal, and spiral fins in both vertical and horizontal orientations for the melting process. The highest melting rate was achieved by the annular fins unit in the vertical orientation and by the longitudinal fins unit in the horizontal orientation.

Other authors have directed their works towards multi-tube systems for enhancing the heat transfer in shell-and-tube LHTES units [16–21]. Joybari et al. [16] experimentally compared the melting and solidification of RT60 in a single tube and multi-tube LHTES unit. Better performance was observed in the multi-tube LHTES unit owing to the increased surface area. Additionally, increasing the flow rate revealed to have no significant enhancement as long as the flow remains turbulent. Kousha et al. [17] experimentally studied the influence of tube number on the melting and solidification of RT35. Four cases with one to four inner tubes were compared. Increasing the number of tubes significantly improved phase change dynamics and increased heat transfer rate. Vikas et al. [18] focused their study on tube arrangement in a five-tube and shell heat exchanger. A 2D numerical simulation was carried out to analyze melting kinetics in ten different arrangements. It was also suggested to place the lower tubes further into the poor melting zone and the top tubes closer to the center. In their two-dimensional numerical simulation of the melting process, Park et al. [19] evaluated both the effect of number and tube arrangement. Their finding revealed that melting time and tube number are not strongly correlated and that increasing tube number is recommended for limited spaces as this can increase energy density. Nevertheless, tube arrangement was found to significantly impact the melting rate. Besides, it was found that the diamond shape outperformed the rectangular shape for quadruple tubes. Pourakabar et al. [20] performed a 2D numerical study on the melting and solidification within a circular and elliptical enclosure with different tube arrangements and numbers. The circular shell with a vertical dual tube and diamond-shaped quadruple tube recorded the lowest melting and solidification times, respectively. Sodhi et al. [21] presented an experimental investigation of a high-temperature LHTES module with 25 HTF tubes and evaluated the influence of operating parameters on melting and solidification. They found that flow rate had a considerable effect up to a threshold, beyond which the improvement became minor. Besides, during solidification, the heat transfer varied significantly along the length of the storage unit.

Agyenim et al. [22] recommended combining longitudinal fins and multiple tubes to improve both charge and discharge dynamics, as they found that multi-tube systems outperformed in melting, and longitudinal fins performed best in the solidification process. From this perspective, Bouhal et al. [23] developed a 2D melting model to compare multi-tube systems with and without fins. The addition of fins has resulted in a 27.24% reduction in melting time. Johar et al. [24] experimentally the performance of an LHTES unit comprising 45 finned tubes for stationary C.I engine exhaust. The developed unit achieved a charging efficiency, recovery efficiency, and energy saving of 69.53%, 38%, and 11.33%, respectively. Niyas et al. [25] developed a lab-scale prototype with 25 finned tubes evaluated at varying operating parameters. The HTF flow rate showed a lower effect on melting and solidification than inlet temperature, and its influence was contingent upon inlet temperature. Dandotiya et al. [26] evaluated in a 2D computational simulation the effect of fin arrangement on PCM melting

rate. The placement of fins vertically and horizontally between the tubes demonstrated superior performance. Khan et al. [27] examined experimentally solidification in a 21-finned tube. Increasing the flow rate diminished discharge time by 24% and raised mean power up to 49.75%. Al-Mudhafar et al. [28] investigated the proposed "webbed tube" heat exchanger's performance using a two-dimensional numerical method. The incorporation of fins into the multi-tube module notably accelerated the melting process. Anish et al. [29] conducted an experimental study on the melting and solidification of erythritol in a finned multi-tube unit with seven HTF tubes and longitudinal fins. They also observed that the flow rate has a minor effect compared to HTF inlet temperature, and its amplitude is inlet temperature dependent. Subsequently, they analyzed in a 2D study [30] the influence of design parameters on melting, which was found to have a significant impact. Using a 3D numerical approach, Abreha et al. [31] evaluated a multi-tube system with 19 pipes supported by four rectangular fins in each. It was noticed that increasing the flow rate improves heat transfer during melting and solidification. Song et al. [32] designed a novel multi-tube latent heat storage system using tree-shaped fins. Their design improved temperature uniformity in the unit and decreased melting time by 80.2% and 34.4%, respectively, compared to fin-less and finned rectangular-shaped multi-tube units. Similarly, Huang et al. [33], in their 3D numerical study, found a reduction of 29.4% and 22.8% in melting and solidification when using tree-fins instead of longitudinal fins. It was noticed that increasing the flow rate improves heat transfer during melting and solidification. In addition to the above studies, the efficiency of the finned multi-tube units was tested by [34–37] but for triplex heat exchanges.

The review of previous works highlights that the combination of multi-tube configurations with various fin designs presents a promising strategy for achieving high-performance latent heat thermal energy storage (LHTES) units. However, the current body of research on this approach remains limited, with insufficient exploration of diverse geometrical configurations, leaving room for more effective and innovative solutions. Specifically, all existing studies focusing on four-tube arrangements [23,26,28,32,33] have been restricted to square-shaped geometries, neglecting alternative configurations such as diamond-shaped tubes. Yet, diamond-shaped configurations have demonstrated superior thermal performance compared to square-shaped tubes in previous investigations involving multiple finless tubes [19,20].

Furthermore, the literature review reveals that most numerical studies on heat transfer enhancement in LHTES units rely on simplified two-dimensional (2D) simulations, overlooking the impact of the third dimension associated with axial temperature gradients in the tubes. To date, and the best of the authors' knowledge, no 3D studies have systematically quantified the effects of three-dimensionality on phase change dynamics. This gap in the literature underscores the need to assess the relevance of adopting a three-dimensional approach over conventional 2D simulations.

To address these gaps, this study proposes a novel finned diamond-shaped multi-tube LHTES unit to enhance heat transfer performance. The study also seeks to quantify the influence of three-dimensional effects on melting and solidification processes, both locally and globally. The proposed design is evaluated through a 3D numerical approach, comparing its performance against a finless reference system under iso-volume phase change material (PCM) conditions. Given the unit's intended application in low-temperature industrial waste heat recovery, erythritol, recognized for its high energy density and widespread use in this temperature range, is selected as the PCM. At the same time, Hytherm 600 thermal oil is the heat transfer fluid (HTF).

A comprehensive analysis of the melting and solidification processes is performed, focusing on liquid/solid volume fractions, temperature distributions, streamline patterns, and heat duty variations. This work not only quantifies the impact of three-dimensional effects on phase change kinetics but also provides insights into the interactions between Reynolds number variations and finned geometrical enhancements. The findings contribute a holistic and practical solution for industrial waste heat recovery applications, offering valuable guidance for the design and optimization of efficient LHTES systems.

2. Physical and mathematical model

2.1. Physical model

Fig. 1 illustrates the LHTES unit investigated in this work. The first configuration designated here as MT-LHTES unit serves as a reference case. It consists of a horizontal multi-tube-and-shell heat exchanger, in which the PCM (Erythriol) is enclosed in a 70 cm length shell with an inner diameter of 14.43 cm and 2 mm thickness. In comparison, the HTF (Hytherm 600) flows through four equidistant tubes diamond-shaped measuring 2 cm in inner diameter and 2 mm in thickness, positioned 5 cm from the center of the heat exchanger and forming a 90° angle to one another.

In the second configuration, designated here as FMT-LHTES, 2 mm thick longitudinal fins interconnecting the tubes and the shell are added to increase the heat surface contact as illustrated in Fig. 1.b. To compare the two configurations at an iso-volume of PCM, the shell's inner diameter is changed to 14.6 cm with a 2 mm thickness. The HTF tubes' dimensions and positions remain the same as in the reference case. Aluminum is used for fins, tubes, and shells.

Owing to the symmetry of the configuration and the physical phenomenon (including natural convection in the PCM) with respect to x axis, only the vertical half of the geometry is simulated, thus saving computational time and resources.

2.2. Physical formulation

In the present study, the 3D numerical simulations were carried out using the commercial CFD code StarCCM+, where flow and heat transfer in the LHTES nits are modeled through the conservation equations (mass and momentum) and the energy equation, respectively. To simplify the problem resolution, various assumptions were considered :

- The HTF s assumed to be incompressible with a laminar flow.
- The liquid PCM flow is laminar, incompressible and unsteady.
- The Boussinesq approximation is considered to take into account natural convection in the numerical model.
- Heat radiation, heat loss to the environment, viscous dissipation, and volume expansion are neglected.
- Conjugate heat flux is considered between HTF, solid parts, and the PCM.
- Tube, shell, and fins are made of the same material, aluminum, which has constant thermophysical properties in the temperature range studied.
- HTF and PCM have constant thermophysical properties, except for PCM's conductivity and heat capacity, which are temperature-dependent as shown in Table 1.

Based on the above assumptions, the governing equations for the PCM can be written as follows:

Mass conservation equation

$$\nabla \cdot \vec{V} = 0 \tag{1}$$

Momentum conservation equation

$$\rho \frac{\partial \vec{V}}{\partial t} + \rho \left(\vec{V} \cdot \nabla \right) \vec{V} = -\nabla P + \mu \nabla^2 \vec{V} + \vec{S}_B + A\vec{V} \tag{2}$$

Energy equation

$$\rho \frac{\partial H}{\partial t} + \rho \nabla \left(\vec{V} \cdot H \right) = \nabla \left(\frac{\lambda}{C_p} \nabla h \right) \tag{3}$$

The term H in the energy equation refers to the total enthalpy per unit mass, calculated as the sum of the sensible heat h per unit mass and the latent content ΔH :

$$H = h + \Delta H \tag{4}$$

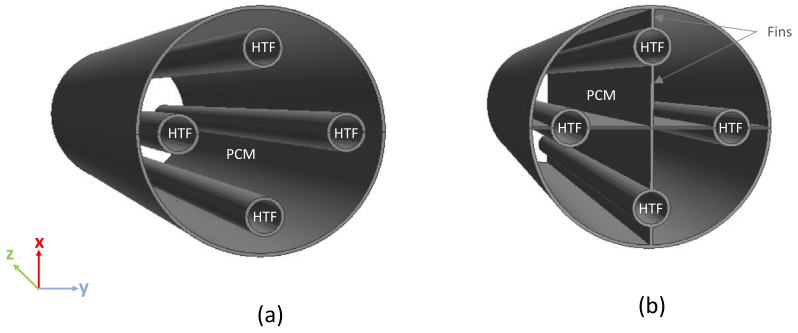

Fig. 1. 3D isometric views of the studied LHTES units : (a) Plain multi-tube configuration (MT-LHTES, reference case), (b) Finned multi-tube configuration (FMT-LHTES unit, enhanced case).

Table 1
Thermophysical properties of PCM (Erythritol), HTF (Hytherm 600) and aluminum [38], [39].

	ρ	μ	λ	C_p	L	T_s	T_l	β
	kg m^{-3}	Pa s	W m^{-1} K^{-1}	J kg^{-1} K^{-1}	kJ kg^{-1}	°C	°C	K^{-1}
PCM	1480 at 20 °C	0.01	0.733 at 20 °C 0.326 at 140 °C linear	solid : 1380 liquid : 2760 linear between T_s and T_l	339.8	116.7	118.7	0.001014
HTF	720.9	19.5×10^{-3}	0.1161	3097.4	–	–	–	–
Aluminum	2719	–	202.4	871	–	–	–	–

$$h = h_{ref} + \int_{T_{ref}}^{T} C_p dT \tag{5}$$

$$\Delta H = f_l \cdot L \tag{6}$$

With f_l is the PCM liquid volume fraction defined as :

$$f_l = \begin{cases} 0 & \text{if } T < T_s \\ \dfrac{T - T_s}{T_l - T_s} & \text{if } T_s < T < T_l \\ 1 & \text{if } T > T_l \end{cases} \tag{7}$$

To model natural convection, a buoyancy source term $\vec{S}_B = \rho \vec{g} \beta \left(T_{ref} - T\right)$ was added to the momentum equation, as well as the source term $A\vec{V}$, which enables modeling all PCM states, solid, liquid, and the so-called mushy zone, characterized by the co-existence of the solid and liquid phases and treated as a porous region. This term is based on the Carman–Kozeny relation :

$$A = -C \frac{(1 - f_l)^2}{f_l^3 + \epsilon} \tag{8}$$

Where C is the mushy zone constant, with recommended values between 10^4 and 10^7 [30]. Therefore, in this study, it is taken as 10^6, the default value in Star CCM+. ϵ is a numerical constant with a very small value to avoid division by zero.

2.3. Initial and boundary conditions

2.3.1. Melting process

To model the melting process, the following initial and boundary conditions are considered :

– Initial condition :

At $t_0 = 0$ s, the PCM is totally solid, and the whole system is considered to have a uniform temperature of 80 °C. This starting temperature is below the melting temperature of the MCP, i.e., a preliminary sensible phase is included in this study.

– Boundary condition :

At the inlet, HTF is assumed to enter the tubes at a uniform temperature of ° C and velocities defined as a Poiseuille profile with bulk velocities of 2.7 m s^{-1} and 1.35 m s^{-1}, corresponding respectively to Reynolds numbers of 2000 and 1000. At the outlet, pressure outlet boundary condition is imposed. As for the fluid–solid and solid–solid interfaces, conjugate heat flux is adopted. Besides, with heat loss being neglected, the outer wall of the heat exchanger is considered adiabatic. Symmetry boundary condition is used through a splitting vertical plane passing across the middle of the LHTES unit.

2.3.2. Solidification process

To model the solidification process, the following initial and boundary conditions are considered :

– Initial condition :

At $t_0 = 0$ s, the PCM is totally liquid, and the whole system is considered to have a uniform temperature of 155 °C, enabling additional sensible heat storage at the beginning. This temperature is chosen in such a way that the difference between the initial temperature and the phase change temperature remains the same in both processes.

– Boundary condition :

For solidification, all boundary conditions remain identical to those corresponding to the above melting process, apart from the HTF inlet temperature, which is brought down to 80 °C.

3. Numerical procedure

3.1. Numerical scheme and solvers

The numerical model was built using the commercial code Star-CCM+, where the governing equations were solved using finite volume discretization and based on the enthalpy porosity method. The conservation equations were consequentially solved by the Algebraic Multigrid (AMG) solver. A segregated flow model was employed using the SIMPLE algorithm for pressure and velocity coupling. A second-order discretization was adopted for convective terms of the momentum and energy equations and temporal discretization.

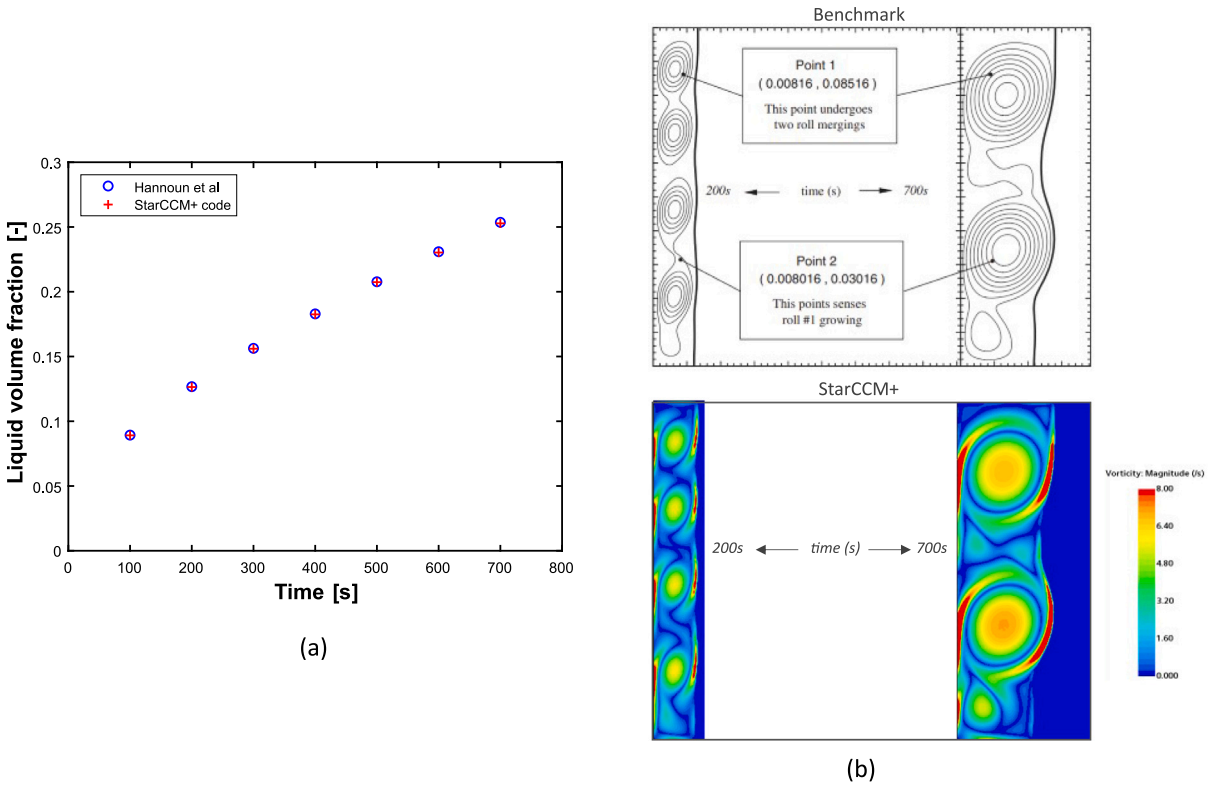

Fig. 2. Validation results : Liquid volume fraction comparison (a), convective cells comparison with Hannoun et al. [40] (b).

3.2. Code validation

A validation study was performed to assess the CFD code accuracy in modeling phase change problems involving natural convection, and the results obtained with the CFD code were compared to the benchmark of Hannoun et al. [40]. The studied problem consists of tin melting in a 0.1×0.1 m square cavity deferentially heated. The system is initially at tin's melting point T_f, then to start melting, the right wall is heated to a temperature $T_h > T_f$. The left wall temperature is kept at $T_c = T_f$, while the top and bottom walls are considered adiabatic. Fig. 2.a compares the benchmark's liquid volume fraction evolution over time with our CFD code. The two studies agree well, with a maximum relative difference of 0.31%.

As tin melts, rolling cells appear, testifying to the presence of natural convection provoked by the temperature gradient between the cavity sides in the presence of gravity. These cells vary in number and size over time. Fig. 2.b shows the convective cells for the benchmark along with our CFD code; where the buoyancy source term is introduced using a field function; at two different times : 200 and 700 s.

The results show that the utilized CFD code reproduces the cell's shape and number, as well as the solid–liquid interface's shape, thus confirming its ability to correctly simulate natural convection in a phase change problem. This was also confirmed previously by Dekhil et al. [41,42] and Kabore et al. [1]. The latter further validated Star CCM+'s accuracy by comparing their data with an experimental study conducted by Longeon et al. [43].

3.3. Grid and time step independence analysis

A grid and time step independence analysis was conducted to determine the optimal grid size and time step, offering a good trade-off between precision and computational time. This was performed for the solidification process on the more complex configuration, the FMT-LHTES unit (the enhanced configuration), and with the highest Reynolds value, 2000.

The trimmer cells meshes of Star CCM+ CFD code, which generates hexahedral cells, were utilized for PCM and HTF tubes, whereas the polyhedral mesh with a thin layer number of 2 was used for the metal regions. Moreover, to perform the grid sensitivity, a selection of five different grid numbers was used, ranging from the most refined, with 4.3 million cells, to the coarsest, with 1 million cells. Fig. 3.a displays the obtained results of heat duty evolution for each cell number (left axis) along with the relative error calculated with respect to the finest cells, i.e., 4.3 million. Besides, Fig. 3.b compares the CFD calculated friction factor in the HTF tubes with the theoretical factor in laminar flow calculated as $\frac{64}{Re}$.

In this study, to maximize the reliability of our simulations, it was decided that the number of grids to be selected should not exceed 1% relative error with respect to the finest mesh. This applies to 3.5 and 2.6 million cells for both heat duty and friction factor, yet the mesh configuration with 2.7 million cells was chosen to save computational time and cost.

Following the above grid sensitivity study, a time-step independence analysis was conducted using the mesh topology chosen earlier. To this end, a set of six different time steps, 0.025 s, 0.05 s, 0.1 s, 0.2 s, 0.4 s, and 0.8 s, with a maximum inner iterations of 100 for each time step. Based on this study, it was decided to adopt a variable step time approach with $\Delta t = 0.025$ s for $0 \text{ s} < t \leq 100$ s, $\Delta t = 0.05$ s for $100 \text{ s} < t \leq 150$ s, $\Delta t = 0.2$ s for $150 \text{ s} < t \leq 250$ s and $\Delta t = 0.4$ s for $t > 250$ s. This will allow to capture high temperature gradient at early stages [42].

4. Results and discussions

This section will present and discuss results from the comparative studies on MT-LHTES and FMT-LHTES units. We will start with a local analysis of melting and solidification mechanisms in both LHTES configurations through the melting/solidification front, streamlines, and temperature evolutions at the transversal middle section. This local analysis will then be extended to other positions to assess the

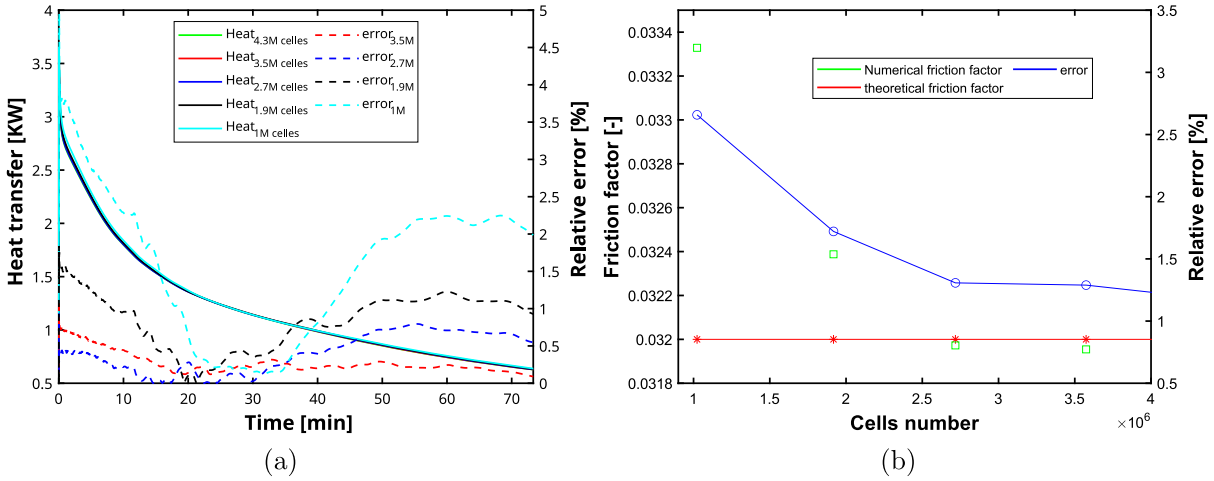

Fig. 3. Grid independence : (a) heat duty evolution over time, (b) friction factor evolution over cells number.

three dimensionality effect related to axial temperature gradient in the tubes. Afterward, a global analysis of liquid/solid volume fraction and heat duty will be presented, allowing a global quantitative assessment of the studied units. The impact of the third dimension will also be quantitatively examined in the same section. This will be followed by an investigation of Reynolds number impact on phase change dynamics. Lastly, further performance analysis will be presented through melting/solidification kinetics and time-average heat duty.

4.1. Local analysis of the melting and solidification processes

4.1.1. Flow structure and temperature fields during the melting process

To visually represent melting dynamics in the plain and finned tubes LHTES units, melting front and streamlines in the transversal middle section are visualized in Fig. 4 at different times: 10, 33, 56, and 73 min. The liquid volume fraction is displayed on the left side, where red and blue colors represent respectively liquid and solid PCM, while the right half shows the streamlines, with white areas referring to solid PCM. In the early stages, a thin layer of liquid PCM forms close to the tubes and fins in the FMT-LHTES unit. This is observed to be symmetrical, indicating a mainly conductive heat transfer at this stage of the melting process. As time passes, liquid proportion increases, and vortices start to form, witnessing the development of natural convection for heat transfer. This leads to an asymmetry in the melt's shape, with more liquid volume fraction in the upper section. This can be explained by buoyancy effects, which, due to density difference, move the warmer PCM upwards and the cooler downwards. Over time, vortices grow, and natural convection becomes more intense, increasing thus the melting speed inside the unit.

The contours overview shows a better distribution of vorticities within the FMT-LHTES (finned configuration) unit. Accordingly, natural convection's influence area expands, reducing total melting time compared to the reference case. In the MT-LHTES unit, the central area experienced a slow melting rate due to its distance from the heating tubes. By installing and extending the fins into the center, this "dead zone" becomes more accessible to the heat, facilitating liquid PCM generation there from an early stage. Moreover, the contribution of fins connecting the tubes to the shell in heat enhancement is not negligible, as it helps to speed up melting around these fins and also enables heating the outer conducting wall, which, by conduction, promotes PCM melting in its vicinity.

Fig. 5 illustrates temperature fields in both MT-LHTES and FMT-LHTES units simultaneously. Heat is transferred from the HTF to the PCM during the melting process due to the temperature gradient. This results in an increase in the temperature of the PCM, followed by a phase change from solid to liquid when its melting temperature is reached. The comparison of the studied LHTES units shows that the specific fins arrangement proposed in this study minimizes the disparity between the upper and lower parts. Additionally, it can be noticed that the FMT-LHTES unit has a higher capacity for storing sensible heat compared to the MT-LHTES unit. This is attributed to extra sensible heat near the fins but primarily to storing sensible heat beneath the splitting horizontal fins, as seen in g and f contours.

Following the local analysis of the melting process and a detailed examination of the underlying physical phenomena using a transversal mid-section, this section explores the longitudinal evolution of the melting process. The objective is to identify potential variations along the third dimension, thereby evaluating the three-dimensional (3D) effects on phase change dynamics. Fig. 6 illustrates the liquid volume fraction contours at three positions along the FMT-LHTES unit: 5, 35 (middle section), and 56 cm and for two different melting times: 56 min and 73 min. The comparison of the liquid volume fraction contours shows a notable difference between the three positions and that for both melting times:

- At t = 73 min, in the section close to the HTF inlet (z=5 cm), only a small amount of PCM remains to be melted which is located at the bottom of the storage unit;
- At a position 30 cm further away (z=35 cm), a larger volume of solid PCM persists in the lower region, indicating a delay in melting compared to the inlet section;
- At z=65 cm, the upper region of the PCM remains partially solid, while the lower region shows an even greater amount of unmelted PCM than the previous sections.

This melting offset between the three positions is attributed to the axial temperature gradient of the HTF, which influences the thermal energy distribution along the unit. However, despite these quantitative differences, the global shape of the melting front remains consistent across the observed sections.

These findings suggest that, while a 2D simplification may provide a reasonable qualitative estimation of the melting front geometry, it would likely result in an inaccurate determination of the liquid volume fraction. The extent of this inaccuracy is expected to increase with the length of the storage unit. In this study, the quantitative impact of these 3D effects will be further analyzed and discussed in a subsequent section.

4.1.2. Flow structure and temperature fields during the solidification process

Fig. 7 presents a combined visualization of liquid volume fraction (left side) and streamlines (right side) within the transversal middle cross-section of both MT-LHTES and FMT-LHTES units at different times (17, 50, 83, and 133 min). The blue and red colors in the liquid volume fraction maps represent the solid and liquid phases,

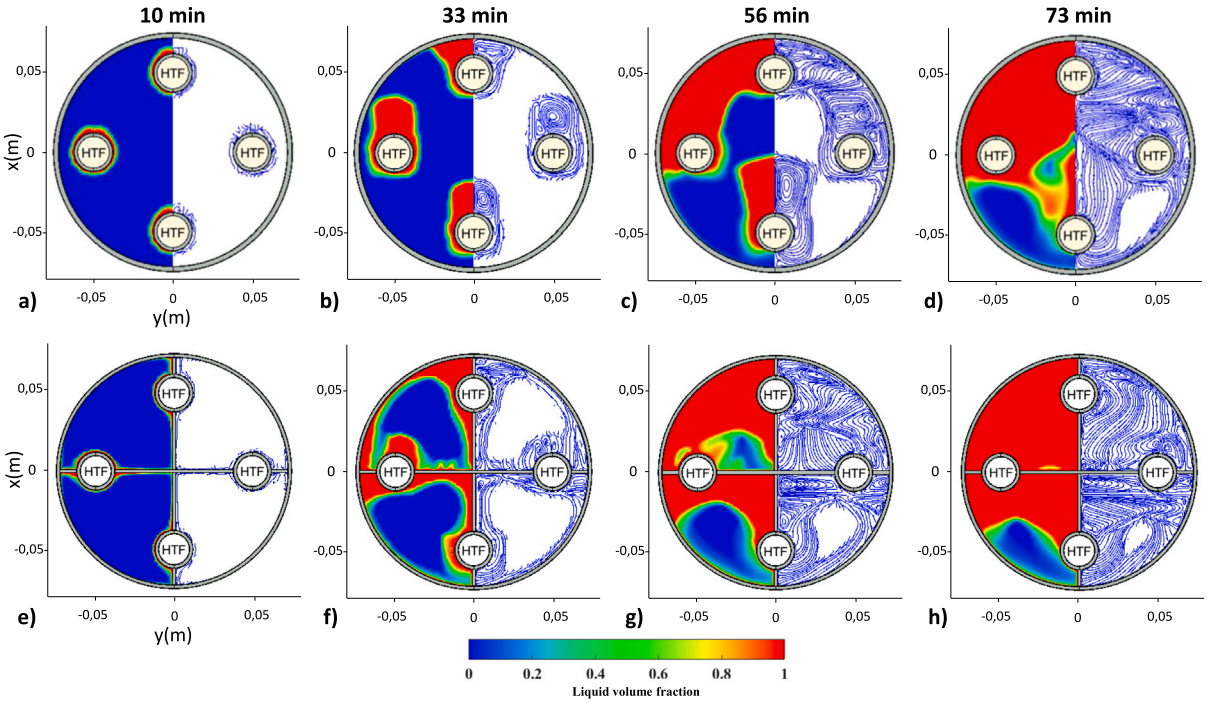

Fig. 4. Liquid volume fraction contours (left half) and flow streamlines (right half) in the PCM for the plain configuration, MT-LHTES unit (a, b, c, d) and the enhanced configuration, FMT-LHTES unit (e, f, g, h) at different instants of melting process.

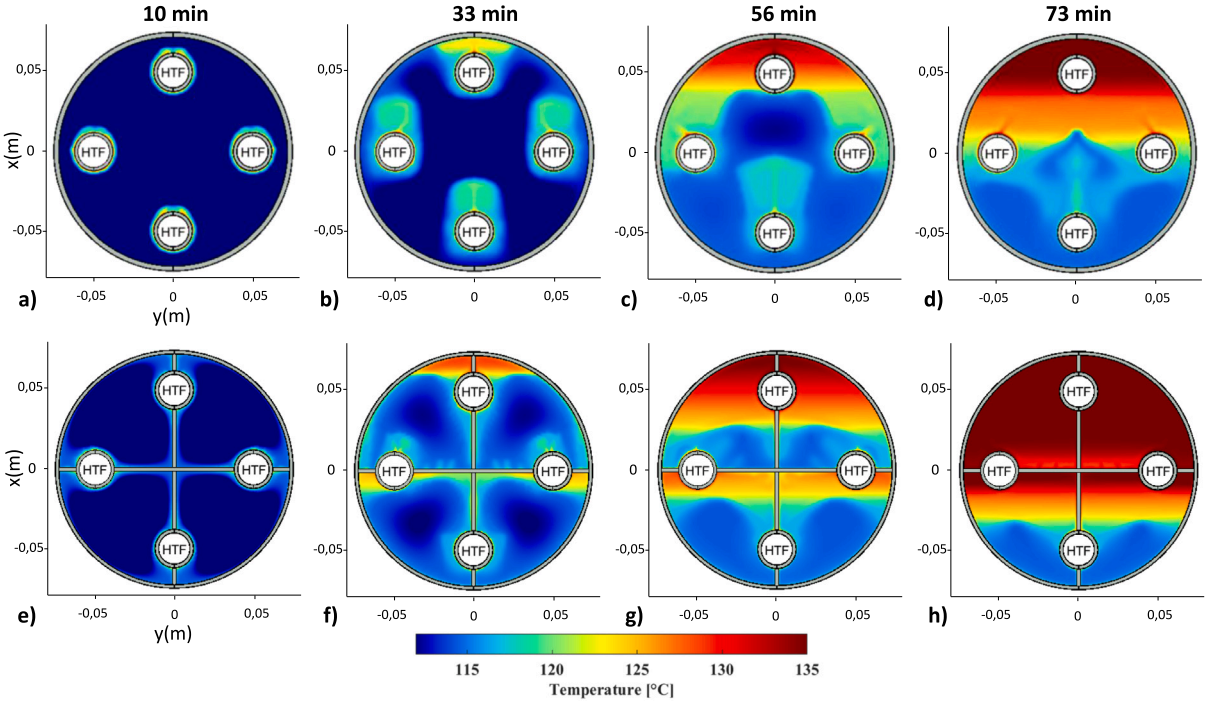

Fig. 5. Temperature fields in the PCM for the plain configuration, MT-LHTES unit (a, b, c, d) and the enhanced configuration, FMT-LHTES unit (e, f, g, h) at different instants of melting process.

respectively. The white areas in the streamlines symbolize the solid phase. In the first stage of the solidification process, natural convection predominates in the heat transfer process, creating an asymmetric solidification front. Buoyancy effects cause the hot PCM to rise and the cold PCM to fall, resulting in a greater amount of solid PCM in the bottom of tubes and the bottom section. As the solidified PCM proportion grows, the natural convection effect decreases along with the vortices size, which relocate far away from cooling sources. This allows conduction to take over as the primary heat transfer mechanism, thus slowing down the solidification rate.

Upon examination of the LHTES units under study, it is clear that solidification is much faster in the FMT-LHTES configuration. Including fins increases the heat exchange surface area, improves heat transfer, and accelerates solidification. Furthermore, by extending fins to the unit center, PCM solidification in this area starts early on, whereas, in the reference case, the center region constitutes a "dead zone"

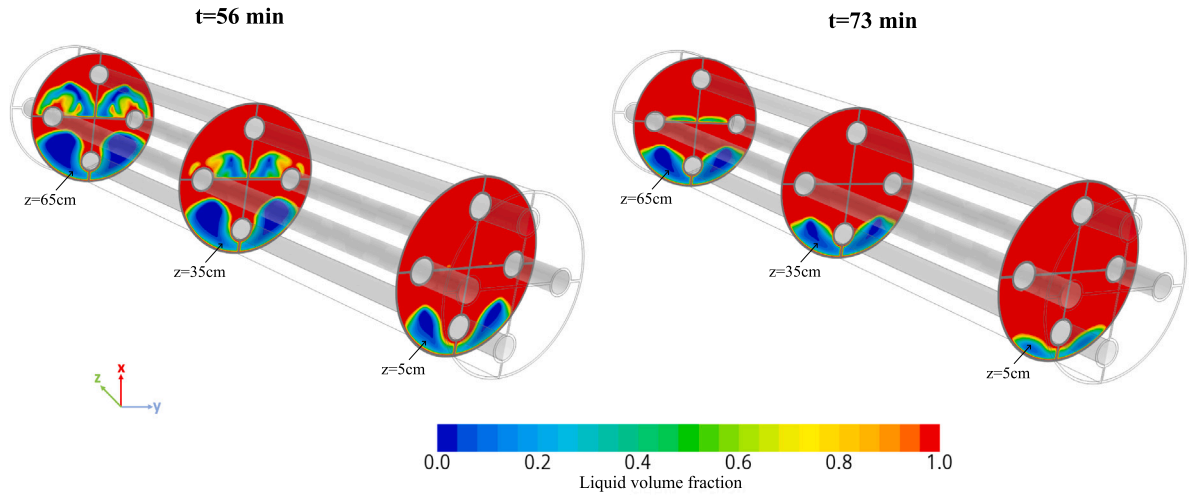

Fig. 6. Liquid volume fraction contours at different positions of the FMT-LHTES unit during melting process.

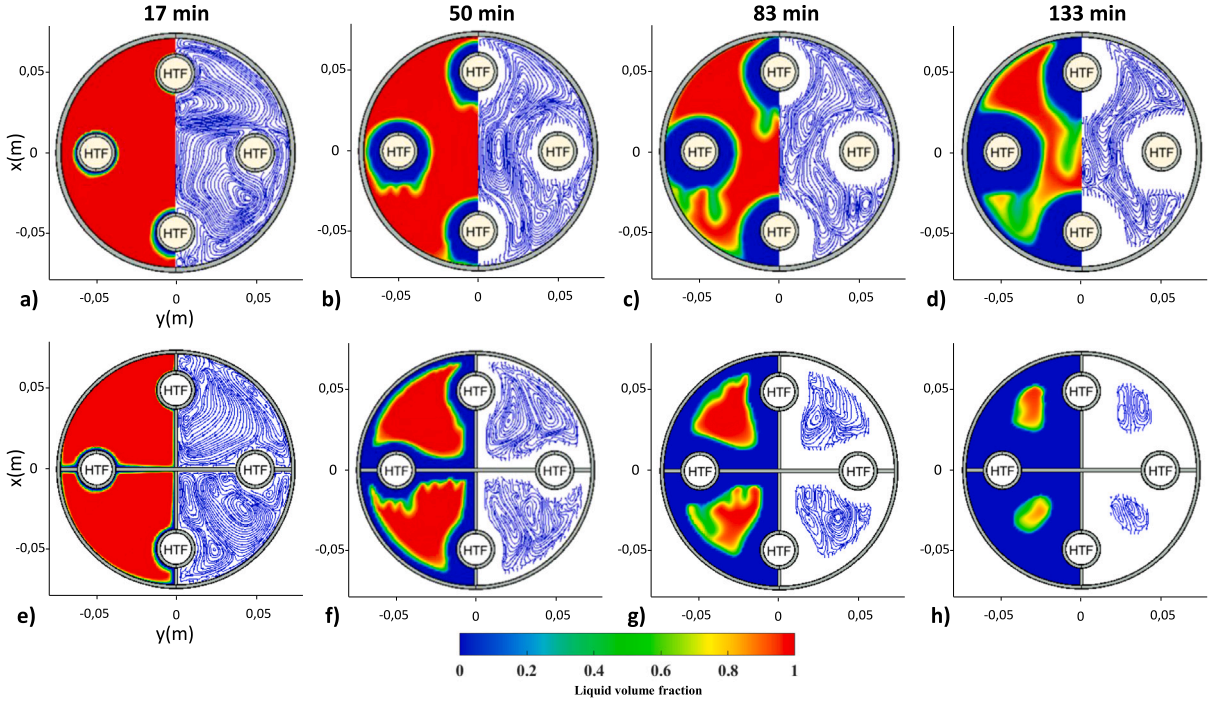

Fig. 7. Liquid volume fraction contours (left half) and flow streamlines (right half) in the PCM for the plain configuration, MT-LHTES unit (a, b, c, d) and the enhanced configuration, FMT-LHTES unit (e, f, g, h) at different instants of solidification process.

requiring considerable time to solidify due to its distance from the tubes. The insertion of fins connecting the tubes and the shell metal surface also contributed to boost solidification in the finned system. Along with extending heat surface contact, the fins also cools down the shell metallic surface, which, through conduction accelerates the solidification in its surrounding.

Fig. 8 illustrates temperature fields during solidification process for the studied LHTES units at different times. During the solidification process, heat is released by the PCM, causing its temperature to drop until it reaches the phase change temperature, after which PCM starts to transform from liquid to solid state. The examination of temperature contours reveals that fins improves temperature uniformity and reduces the temperature gradient between the top and the bottom of the storage unit. Moreover, it can be observed that FMT-LHTES unit not only stores sensible heat around the HTF tubes, but also stores additional sensible heat in the vicinity of the fins and the conducting wall. This results in a higher total stored heat in the FMT-LHTES unit compared to the MT-LHTES unit.

Similar to the melting process analysis, the three-dimensionality effect is now evaluated during the discharge (solidification) process. Fig. 9 presents the liquid volume fraction contours at three longitudinal positions along the FMT-LHTES unit: z = 5 cm, z = 35 cm, and z = 65 cm, at two distinct time points: 83 min and 133 min. For both time instances, it is evident that the axial temperature gradient of the heat transfer fluid (HTF) along the storage unit significantly affects the solidification rate:

- Near the HTF inlet (z = 5 cm), the solidification process occurs more rapidly than in downstream sections. This faster solidification is attributed to the lower HTF temperature at the inlet, which creates a higher thermal gradient and thus intensifies heat exchange with the phase change material (PCM).

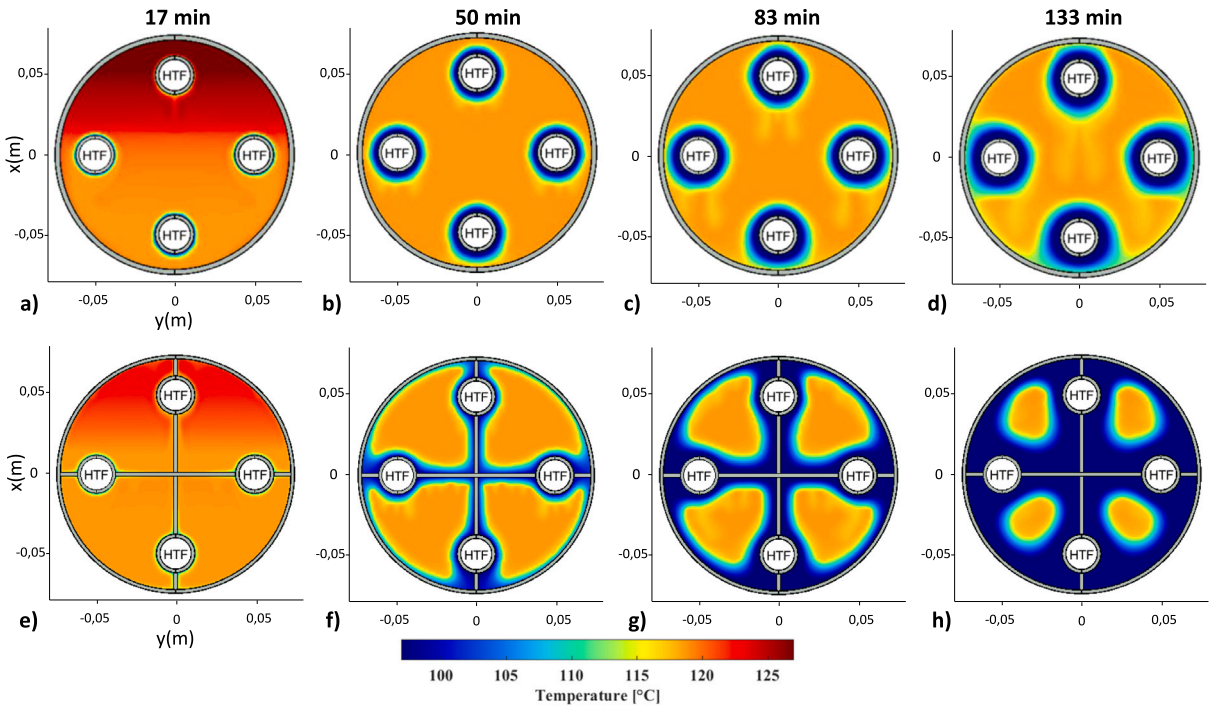

Fig. 8. Temperature fields in the PCM for the plain configuration, MT-LHTES unit (a, b, c, d) and the enhanced configuration, FMT-LHTES unit (e, f, g, h) at different instants solidification process.

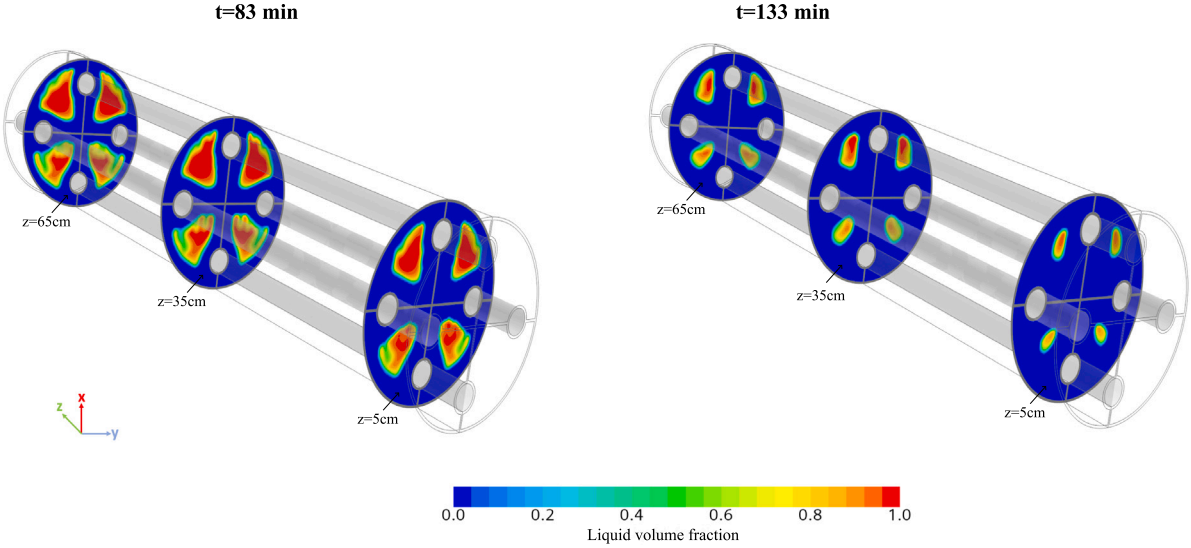

Fig. 9. Liquid volume fraction contours at different positions of the FMT-LHTES unit during solidification process.

- Moving downstream, at z = 35 cm and z = 65 cm, the HTF temperature gradually increases, leading to a reduced thermal gradient and, consequently, slower solidification rates. The amount of solidified PCM decreases further from the inlet, reflecting the diminishing heat transfer efficiency along the unit's length.

Interestingly, despite these variations in solidification rates, the overall shape of the solidification front remains consistent across all positions. This observation indicates that while the axial temperature gradient influences the speed of solidification, it does not alter the geometric profile of the solidification front.

To quantitatively assess the impact of the third dimension, a detailed analysis will be presented in a subsequent section, providing insights into the significance of 3D effects on the solidification process within the FMT-LHTES unit.

4.2. Global analysis of the melting and solidification processes

4.2.1. Melting process

To quantify the phase change during the melting process, the volume average liquid volume fraction variation over time for the MT-LHTES and FMT-LHTES units are illustrated in Fig. 10. In the first nine minutes, PCM melts faster in the reference case, MT-LHTES unit. Fins efficiency is not instantaneous as they must be heated first, utilizing a portion of the heat for this purpose. This reduces the amount of heat transferred to the PCM, hence, delaying its melting. However, once heated, the fins' efficiency starts to show through accelerating PCM melting. In the finned-tube configuration FMT-LHTES unit, complete melting is reached at 106.87 min (1h 46 min) rather than 124.3 min (2h

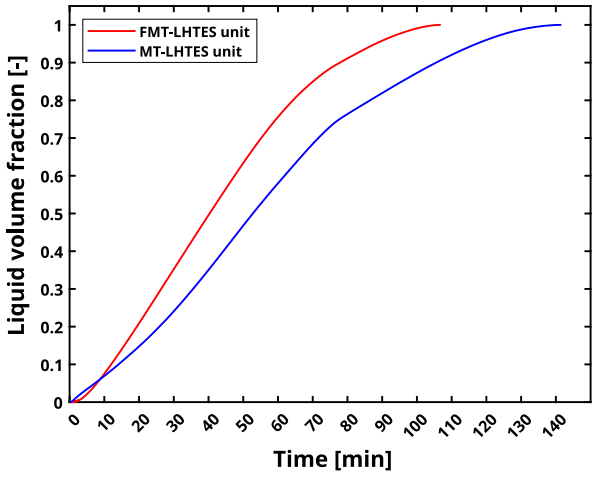

Fig. 10. Temporal evolution of liquid volume fraction during the melting process in both MT-LHTES and FMT-LHTES units.

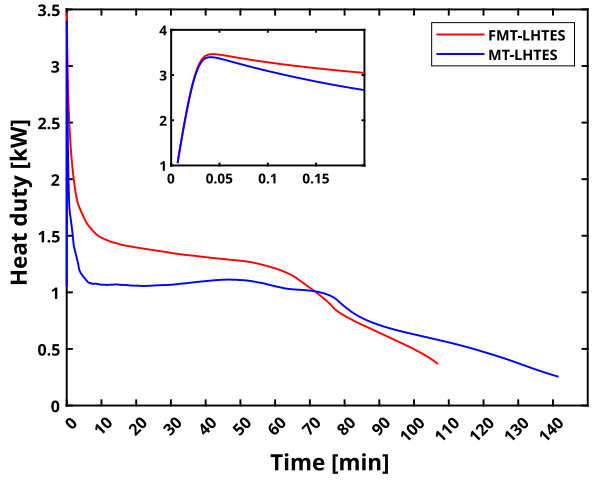

Fig. 11. Temporal evolution of heat duty during the melting process in both MT-LHTES and FMT-LHTES units.

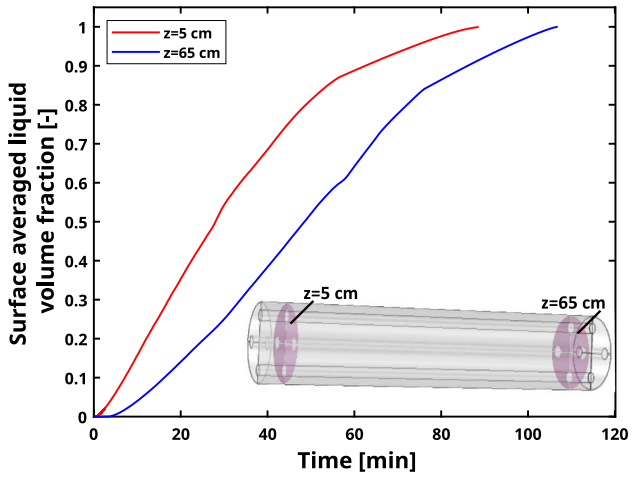

Fig. 12. Transient liquid volume fraction during the melting at two positions from the HTF inlet of the FMT-LHTES unit.

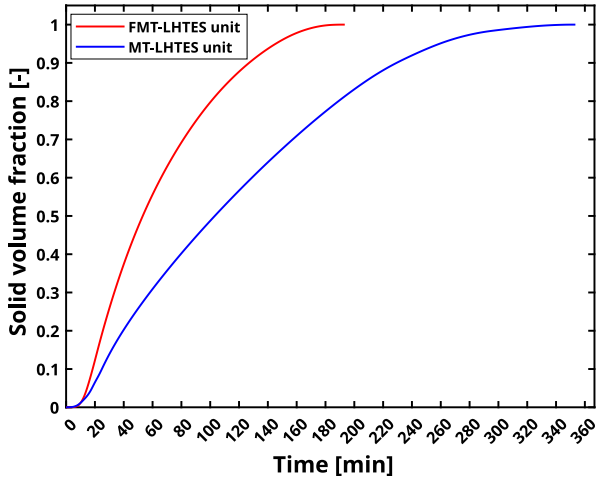

Fig. 13. Temporal evolution of solid volume fraction during the solidification process in both MT-LHTES and FMT-LHTES units.

22 min) in the reference case without fins, leading to a 24.5% reduction in melting time.

A heat-duty over time comparison between finned and fin-less systems is depicted in Fig. 11. It is worth noting that the represented heat duty is the sum of all tubes calculated at the HTF interface. Due to the high temperature gradient at the beginning, a sharp increase of heat duty is observed, reaching maximum values of 3.46 and 3.4 kW for the FMT-LHTES and MT-LHTES, respectively. As melting proceeds, the temperature gradient between the PCM and the HTF decreases, resulting in a drop in the exchanged heat duty. It can be observed that the heat transfer is more efficient when fins are installed, explaining faster melting in this case. When melting reaches an advanced stage, the amount of heat exchanged decreases considerably. This explains the lower heat duty after 70 min in the enhanced configuration (already at 85% melting) compared to the reference case, which is still at a less advanced stage of melting (71%).

To quantitatively evaluate the axial temperature gradient effect on the melting process, the temporal evolution of the transversal surface average liquid volume fraction in two different positions on the length of the FMT-LHTES unit is illustrated in Fig. 12. For this study, positions are chosen as 5 cm from the HTF inlet (z=5 cm) and 5 cm away from the HTF outlet (z=65 cm). A significant difference can be observed in the evolution of the surface average liquid volume fraction between these positions. As expected and as observed in the local liquid volume fraction contours, PCM near the HTF inlet melts faster than that near the outlet. An 18.2 min difference is recorded in the full melting time, with 88.64 min (1h 29 min) at z=5 cm and 106.84 min (1h 47 min) at z=65 cm. This demonstrates that axial temperature gradient effect on melting dynamics is not negligible (in this case study with a 70 cm length and in which the HTF flow is also modeled) and is clearly important to the unit's performance.

4.2.2. Solidification process

To compare solidification dynamics between MT-LHTES and FMT-LHTES units on a global point of view throughout the entire unit, variation over time of volume average solid volume fraction is plotted in Fig. 13, with solid volume fraction $f_s = 1 - f_l$. The obtained results show a pronounced disparity in solid volume fraction evolution between both configurations. The FMT-LHTES unit starts slightly slower than the MT-LHTES unit, owing to the required cooling of the fins, but its performance increases thereafter and exhibits considerably faster solidification. Complete solidification occurs after 353 min (5h 53 min) in the MT-LHTES unit. However, adding fins shorten this time to 192.44 min (3h 12 min), indicating a 45.5% reduction in solidification time.

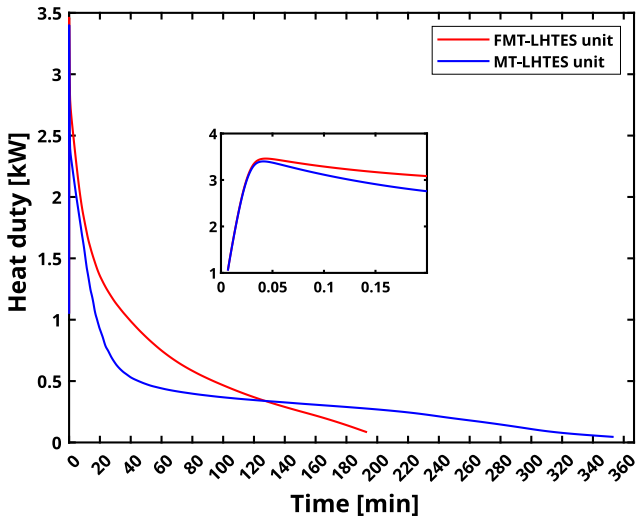

Fig. 14. Temporal evolution of heat duty during the solidification process in the MT-LHTES and FMT-LHTES units.

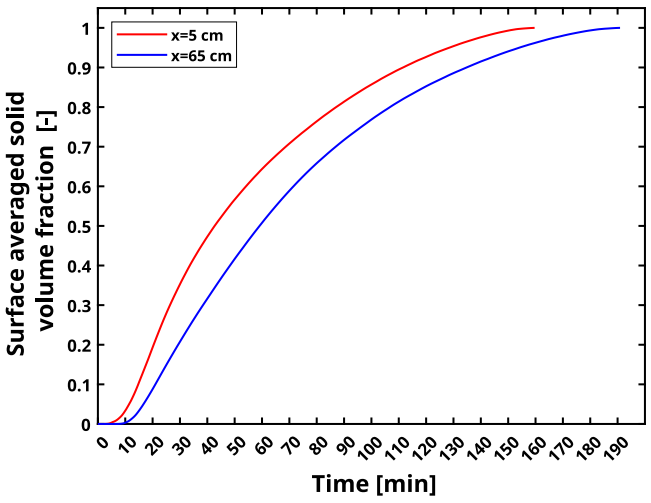

Fig. 15. Transient solid volume fraction during solidification at two positions from the HTF inlet of the FMT-LHTES unit.

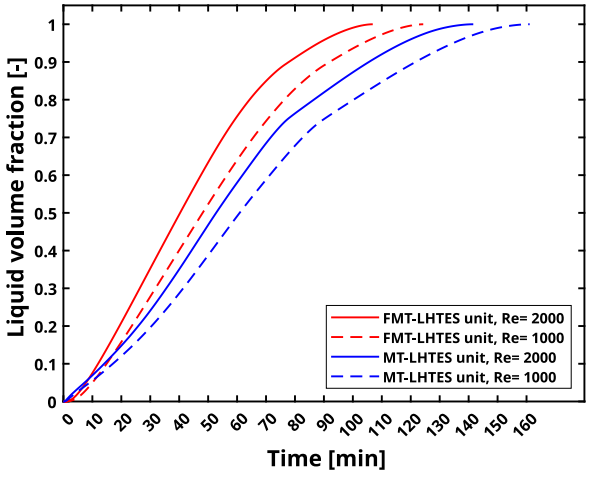

Fig. 16. Evolution with respect to time of the liquid volume fraction during melting for Reynolds numbers of 1000 and 2000 in both configurations.

For a more in-depth comparison, the heat duty temporal evolution of both configurations during solidification is depicted in Fig. 14. The represented heat duty is determined at the HTF interface by summing the values of each tube. A peak is observed at the beginning owing to the significant temperature gradient between the PCM and the HTF. After reaching peak values of 3.46 and 3.4 kW for FMT-LHTES and MT-LHTES units, the exchanged heat gradually decreases due to temperature gradient drop. The results from Figs. 13 and 14, confirm the correlation between adding fins, increasing heat transfer, and accelerating PCM solidification. This is supported by the fact that the FMT-LHTES unit has higher heat duty and faster solidification when compared to the MT-LHTES unit.

Fig. 15 illustrates solid volume fraction evolution over time in the FMT-LHTES unit at two positions from the HTF inlet z=5 cm and z=65 cm. This enables the evaluation of the impact of the axial temperature gradient on the solidification process and the assessment of the relevance of adopting a 3D model instead of a 2D modeling approach. As can be seen, there is a noticeable difference between the curves, with faster solidification at all times near the inlet, as predicted. 16.36% difference is noted between the two positions when complete solidification in these planes is reached, giving that PCM in the transversal plane located at z=5 cm fully solidifies after 159.66 min (2h 40 min), while in the plane located at z=65 cm it takes 190.9 min (3h 11 min). This difference is not negligible, especially if a proper estimation of solidification dynamics is desired, in which case a 3D approach should be adopted.

4.3. Effect of Reynolds number on the melting and solidification processes

This section is devoted to examining the effect of Re number on melting and solidification dynamics. To this end, numerical simulations have been performed using two Reynolds numbers: 1000 and 2000, respectively, corresponding to 2.7 and 1.35 m/s HTF bulk velocities in the Poiseuille flow imposed at the inlet. Reynolds number defined as :

$$Re = \frac{\rho \times U \times D}{\mu} \tag{9}$$

With U the HTF bulk velocity and D the internal tube diameter.

4.3.1. Effect of re number on the melting process

Fig. 16 presents the evolution of the liquid volume fraction for both Reynolds numbers: Re = 2000 (solid lines) and Re = 1000 (dashed lines) and for both MT-LHTES and FMT-LHTES units. It can be observed from these results that, for both configurations, the higher Re number exhibits a shorter melting time at all times, with a noteworthy difference from the lower Re number. This difference for full melting time is slightly higher in the enhanced case, and it is on the order of 14% and 12.1% for FMT-LHTES and MT-LHTES units, respectively. The complete melting time for each case is reported in the Table 2.

The acceleration of the melting process when increasing the Reynolds number results from the heat transfer enhancement as shown in Fig. 17 representing heat duty evolution. A higher heat transfer rate is observed with a higher Re number for both configurations. The relationship between Re number and heat duty can be explained by the fact that increasing Reynolds number leads to an increase of convective heat transfer coefficient inside the HTF tube, this in return induces a higher heat transfer rate at the wall interface and accelerate melting process. It should be noted that this proportionality is not linear. In simpler terms, doubling the Reynolds number does not necessarily result in a doubling of heat transfer. For instance, when considering the maximum heat duty (see Table 2), a Reynolds number ratio of 2 leads

Table 2
Complete melting time and maximum heat duty for both FMT-LHTES and MT-LHTES units during melting process.

	FMT-LHTES unit		MT-LHTES unit	
	Re = 2000	Re = 1000	Re = 2000	Re = 1000
Complete melting time (min)	106.87	124.31	141.6	161.08
Maximum heat duty (kW)	3.46	2.7	3.39	2.63

Table 3
Complete solidification time for both FMT-LHTES and MT-LHTES units.

	FMT-LHTES unit		MT-LHTES unit	
	Re = 2000	Re = 1000	Re = 2000	Re = 1000
Complete solidification time (min)	192.44	209.31	353.04	364.08

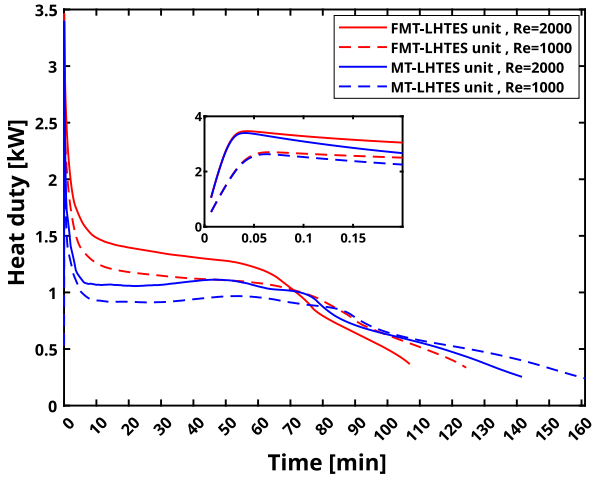

Fig. 17. Evolution with respect to time of the heat duty during melting for Reynolds numbers of 1000 and 2000 in both configurations.

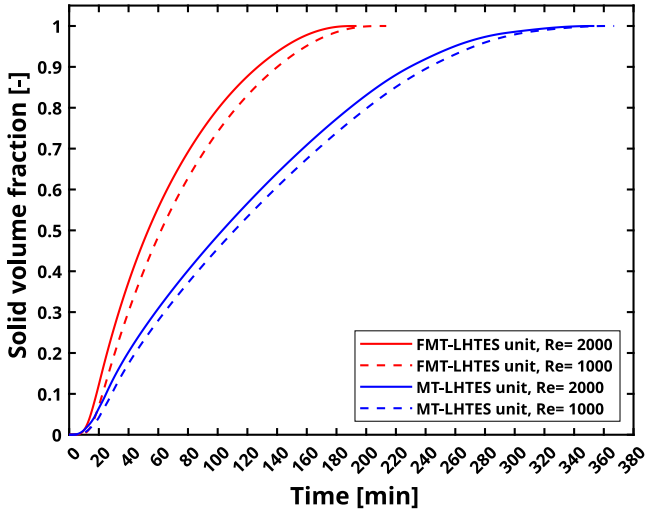

Fig. 18. Transient solid volume fraction during solidification for Reynolds numbers of 1000 and 2000 in both configurations.

to nearly similar heat duty ratios of 1.28 and 1.29 for both FMT-LHTES and MT-LHTES units, respectively.

4.3.2. Effect of Re number on the solidification process

To examine the Re numbers effect on solidification dynamics, solid volume fraction evolution over time for the enhanced and reference cases and for Reynolds numbers 2000 (solid lines) and 1000 (dashed lines) is displayed in Fig. 18. A difference in phase change evolution is also noted between both Reynolds numbers during the solidification process, with higher values of solid volume fraction at higher Re number. Yet, this difference is minor in the MT-LHTES unit and is of the order of 3% when considering the complete solidification time (see Table 3), compared with 8% for the FMT-LHTES unit. Thus, in the solidification process, the effect of the Reynolds number is highly dependent on the intensification in the PCM side.

For a more comprehensive analysis, heat duty evolution during solidification is represented in Fig. 19. For the FMT-LHTES unit, the increase in Reynolds number leads to an increase in heat duty and, consequently, a relevant reduction in solidification time. However, in the MT-LHTES unit, there is no significant difference between the two Reynolds numbers, resulting in close values of total solidification time for Re=2000 and Re=1000.

During solidification, where conduction controls heat transfer on the shell side, the limited heat exchange surface area in the reference unit reduces the influence of the intensified convection on the HTF side. So, even with a higher Reynolds number, the improvement in heat transfer remains limited. In contrast, in the FMT-LHTES unit, the increase in the heat exchange surface created by adding fins makes the influence of Reynolds number – and therefore the improvement in convection in the tubes – more pronounced.

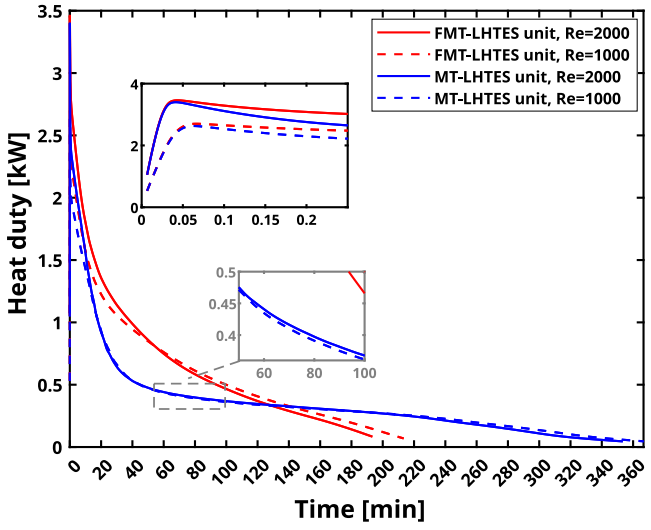

Fig. 19. Evolution with respect to time of the heat duty during solidification for Reynolds numbers 1000 and 2000 in both configurations.

4.4. Performance analysis of the LHTES unit

This section uses the melting/solidification kinetics and the time-average heat duty as performance indicators to further evaluate the proposed LHTES unit. Its performance is also compared with that of the reference case for Reynolds numbers 1000 and 2000.

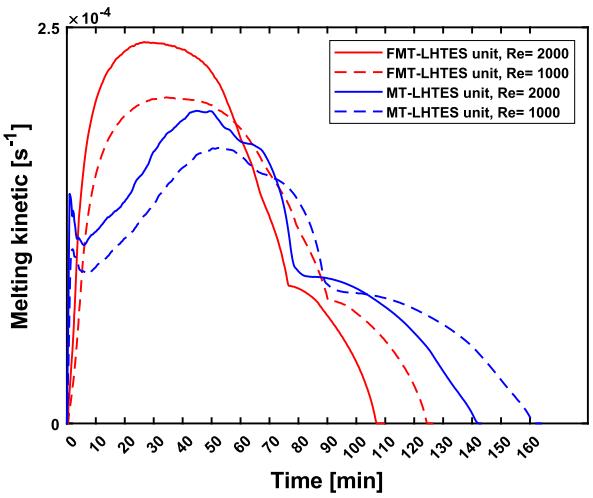

Fig. 20. Melting kinetic evolution in both configurations for Reynolds numbers of 1000 and 2000.

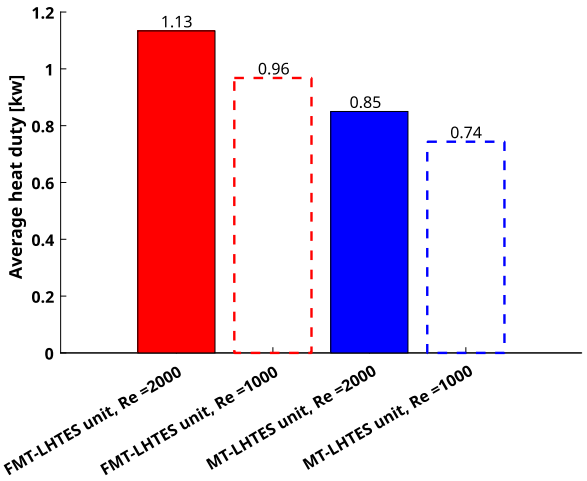

Fig. 21. Time-average heat duty for both FMT-LHTES and MT-LHTES units with Reynolds numbers of 1000 and 2000 during melting process.

The melting/solidification kinetic represents the phase change velocity at each time step and is computed as follows:

$$V_{l/s} = \frac{df_{l/s}}{dt} \tag{10}$$

As for the time-average heat duty, it is determined from the start of the process to total melting/solidification. It, therefore, includes the preliminary sensible heat and latent heat. The average heat duty is calculated as follows:

$$Po_{average} = \frac{1}{t_{full} - t_0} \int_{t_0}^{t_{full}} Po(t)dt \tag{11}$$

4.4.1. Melting process

Fig. 20 displays the time melting kinetic with respect to time for both MT-LHTES and FMT-LHTES units with Reynolds values of 1000 and 2000. Overall, the different cases first show an increase in melting kinetic due to the acceleration of natural convection over time. This increase continues until reaching a peak value, at which point the melting rate starts to decrease as the end of the phase change approaches. This deceleration is attributed to the minimum temperature difference between PCM and HTF at this final melting stage. While the general patterns are similar in all cases, they differ in terms of their level of variation. With the same Reynolds number, a sharper increase with higher melting kinetic values is observed in the FMT-LHTES compared to the MT-LHTES unit. This reflects higher natural convection intensity and rapid melting in the first case. Furthermore, the analysis of Reynolds number indicates that liquid PCM development occurs more rapidly and at higher speeds with greater Reynolds numbers. This figure also demonstrates that the enhancement from the PCM side using fins has a more significant effect than the enhancement from the HTF side by increasing the Reynolds number.

The global melting performance evaluation through average heat duty is illustrated in Fig. 21. It can be observed that from the beginning of the PCM heating process, where the heat is first transferred in sensible form followed by the latent form until the full-time melting, a time-average heat duty of 1.13 kW was exchanged in the FMT-LHTES unit with a Reynolds number of 2000, which is the highest in all cases. Lowering the Reynolds number to 1000 in the FMT-LHTES unit decreases the time-average heat duty by 15%. This reduction is much more significant for the FMT-LHTES unit and Re=2000 when no fins are used (MT-LHTES unit), with a difference of 24.77 for a Reynolds number of 2000 and 34.51 for a Reynolds number of 1000. It is, therefore, of great interest to combine the improvement in heat transfer on the PCM and HTF sides by using fins with high values of Reynolds numbers to significantly improve heat transfer.

4.4.2. Solidification process

Fig. 22 depicts the time-average solidification kinetic evolution over time for both MT-LHTES and FMT-LHTES units and Reynolds numbers of 1000 and 2000. Initially, it can be seen that the solidification kinetic increases until it reaches a maximum value, owing to the natural convection that predominates heat transfer at the early stages of the solidification process and increases over time until a maximum value. The solidification kinetic decreases as conduction becomes predominant in the heat transfer process, and the thermal resistance of the solidified layer becomes higher. When comparing the FMT-LHTES and MT-LHTES units, the latter exhibits lower solidification kinetic as PCM solidifies slowly. Besides, higher solidification speed values are observed with a Reynolds number of 2000 for the FMT-LHTES unit and closed values between the two Reynolds numbers for the MT-LHTES unit.

For an overall assessment of the solidification kinetic, the time-averaged solidification kinetic were calculated. It reaches values of 0.86×10^{-4} s^{-1} and 0.47×10^{-4} s^{-1} respectively for FMT-LHTES and MT-LHTES units for Reynolds of 2000, while lower values of 0.79×10^{-4} s^{-1} and 0.45×10^{-4} s^{-1}, respectively are reached for the Reynolds of 1000. This confirms that the influence of the Reynolds number is dependent on the studied configuration. Moreover, as with the melting process, the enhancement is much more significant from the PCM than the HTF side. Fig. 23 presents the time-average heat duty during the solidification process for both configurations and Reynolds numbers. It should be noted that the given values correspond to average values from the beginning of the PCM solidification process, where the heat is first extracted from the PCM in sensible form, followed by the latent form until the full-time solidification. The highest time-average heat duty is observed in the enhanced case (FMT-LHTES unit) from both PCM and HTF sides by installing fins and using a high Reynolds number of 2000, leading to a value of 0.66 kW. The reduction of the Reynolds number to 1000 decreases the time-average heat duty by 9.1%, while the absence of fins results to more significant decrease of 46.9% and 48.5% for Reynolds number of 2000 and 1000 respectively, with respect to the FMT-LHTES unit with Reynolds number of 2000.

5. Conclusions

This paper presented a comprehensive 3D numerical study evaluating the performance of a novel finned diamond-shaped multi-tube latent heat thermal energy storage (LHTES) unit during melting and solidification processes. Unlike conventional square-shaped designs, the proposed configuration introduces a diamond-shaped multi-tube arrangement embedded with longitudinal fins, providing a new approach to enhancing heat transfer efficiency.

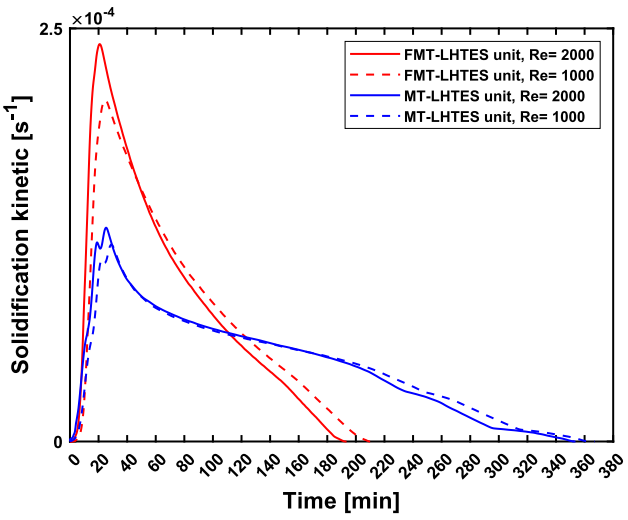

Fig. 22. Solidification kinetic evolution in both configurations for Reynolds numbers of 1000 and 2000.

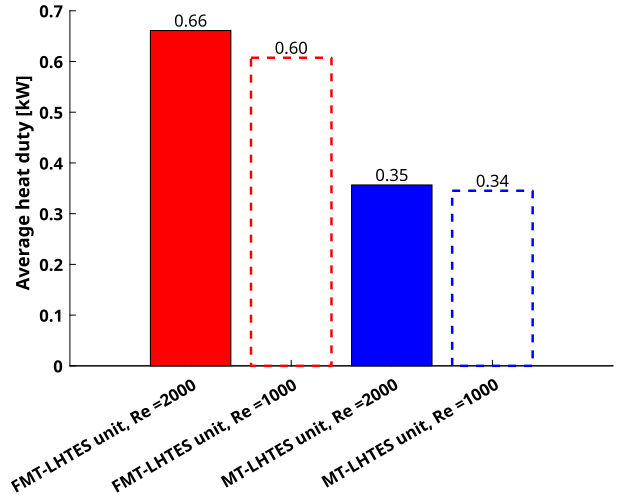

Fig. 23. Time-average heat duty for both FMT-LHTES and MT-LHTES units with Reynolds numbers of 1000 and 2000 during the solidification process.

A comparative analysis was conducted using an iso-volume phase change material (PCM) reference case without fins to assess the impact of the innovative geometry and fin integration. Additionally, the axial temperature gradient was examined to establish the necessity of a three-dimensional (3D) modeling approach over the traditionally employed two-dimensional (2D) methods. A parametric study on the Reynolds number (Re) was also performed to explore its influence on phase change dynamics. The following key findings and original contributions were identified:

- The proposed finned diamond-shaped multi-tube LHTES unit demonstrated superior performance compared to the reference case without fins. The unique diamond-shaped configuration, combined with deeper fin embedding in the PCM, resulted in significant reductions in melting and solidification times by 24.5% and 45.5%, respectively. This confirms that geometric optimization, particularly diamond-shaped arrangements, enhances phase change kinetics and improves thermal performance.
- For the 70 cm long 3D unit, the axial temperature gradient was found to have a non-negligible impact on phase change processes. Differences exceeding 17% for melting and 16.36% for solidification were observed, emphasizing that 3D modeling is crucial for achieving accurate simulation results, particularly for elongated LHTES units. This study provides quantitative evidence supporting the adoption of 3D approaches in future LHTES designs.
- The effect of the Reynolds number is dependent on the phase change (melting or solidification) and the geometrical configuration. - During the melting process, in which convection drives heat transfer, the influence of Reynolds number was slightly greater in the enhanced unit, with a 14% reduction in melting time when the Reynolds number was increased from 1000 to 2000, compared with 12.1% for the reference unit. - During solidification, heat transfer is primarily by conduction, reducing the Reynolds number's impact compared to the melting process. The effect of increasing the Reynolds number was only significant in the enhanced configuration through surface extension using fins. In the FMT-LHTES unit, an 8% reduction in solidification time was achieved by raising the Reynolds number from 1000 to 2000. In contrast, in the MT-LHTES configuration, the limited exchange surface restricted the impact of the Reynolds number to only 3%.
- A synergistic enhancement was achieved by combining heat transfer improvements from the PCM side (via fin integration) with HTF-side enhancements (through increased Reynolds number). This dual strategy substantially improved average heat duty by 34.51% during melting and 48.5% during solidification.

Building upon these findings, the study proposes the integration of vortex generators in the finned multi-tube LHTES unit (FMT-LHTES) as a future research direction. Such integration is expected to further enhance heat transfer on the HTF side, providing a more comprehensive solution for industrial waste heat recovery applications. This work offers a scalable and high-performance LHTES solution and lays the foundation for future innovations in geometry optimization, 3D modeling, and combined enhancement techniques for thermal energy storage systems.

CRediT authorship contribution statement

Soumaya Sokakini: Conceptualization, Methodology, Software, Validation, Formal analysis, Investigation, Data curation, Writing – original draft, Writing – review & editing, Visualization. **Jules Voguelin Simo Tala:** Conceptualization, Methodology, Software, Validation, Formal analysis, Investigation, Data curation, Writing – review & editing, Visualization, Supervision. **Lionel Nadau:** Conceptualization, Methodology, Validation, Formal analysis, Investigation, Data curation, Writing – review & editing, Visualization, Supervision. **Adrian Ilinca:** Conceptualization, Methodology, Validation, Formal analysis, Investigation, Data curation, Writing – review & editing, Visualization, Supervision. **Daniel Bougeard:** Conceptualization, Methodology, Validation, Formal analysis, Investigation, Data curation, Writing – review & editing, Visualization, Supervision.

Declaration of competing interest

The authors declare that they have no known competing financial interests or personal relationships that could have appeared to influence the work reported in this paper.

Acknowledgments

This study was performed with the financial support of ENGIE SA and the Haut-de-France region (HDF) to whom we express our sincere thanks.

Data availability

Data will be made available on request.

References

[1] A. Kaboré, J.V. Simo Tala, Z. Younsi, D. Bougeard, Numerical analysis and optimization of the heat transfer enhancement from the heat transfer fluid side in a shell-and-tube latent heat thermal energy storage unit: Application to buildings thermal comfort improvement, J. Energy Storage 74 (2023) 109530.

[2] Y. Cui, C. Liu, S. Hu, X. Yu, The experimental exploration of carbon nanofiber and carbon nanotube additives on thermal behavior of phase change materials, Sol. Energy Mater. Sol. Cells 95 (4) (2011) 1208–1212.

[3] J. Wang, H. Xie, Z. Xin, Y. Li, L. Chen, Enhancing thermal conductivity of palmitic acid based phase change materials with carbon nanotubes as fillers, Sol. Energy 84 (2) (2010) 339–344.

[4] W.-L. Cheng, W.-W. Li, Y.-L. Nian, W.-d. Xia, Study of thermal conductive enhancement mechanism and selection criteria of carbon-additive for composite phase change materials, Int. J. Heat Mass Transfer 116 (2018) 507–511.

[5] A. Hussain, C.Y. Tso, C.Y.H. Chao, Experimental investigation of a passive thermal management system for high-powered lithium ion batteries using nickel foam-paraffin composite, Energy 115 (2016) 209–218.

[6] T.X. Li, D.L. Wu, F. He, R.Z. Wang, Experimental investigation on copper foam/hydrated salt composite phase change material for thermal energy storage, Int. J. Heat Mass Transfer 115 (2017) 148–157.

[7] K. Yuan, H. Wang, J. Liu, X. Fang, Z. Zhang, Novel slurry containing graphene oxide-grafted microencapsulated phase change material with enhanced thermo-physical properties and photo-thermal performance, Sol. Energy Mater. Sol. Cells 143 (2015) 29–37.

[8] J.N.W. Chiu, V. Martin, Multistage latent heat cold thermal energy storage design analysis, Appl. Energy 112 (2013) 1438–1445.

[9] R. Karami, B. Kamkari, Investigation of the effect of inclination angle on the melting enhancement of phase change material in finned latent heat thermal storage units, Appl. Therm. Eng. 146 (2019) 45–60.

[10] X. Yang, Z. Lu, Q. Bai, Q. Zhang, L. Jin, J. Yan, Thermal performance of a shell-and-tube latent heat thermal energy storage unit: Role of annular fins, Appl. Energy 202 (2017) 558–570.

[11] M. Kirincic, A. Trp, K. Lenic, Numerical evaluation of the latent heat thermal energy storage performance enhancement by installing longitudinal fins, J. Energy Storage 42 (2021) 103085.

[12] Y. Yuan, X. Cao, B. Xiang, Y. Du, Effect of installation angle of fins on melting characteristics of annular unit for latent heat thermal energy storage, Sol. Energy 136 (2016) 365–378.

[13] Z. Liu, Z. Liu, J. Guo, F. Wang, X. Yang, J. Yan, Innovative ladder-shaped fin design on a latent heat storage device for waste heat recovery, Appl. Energy 321 (2022) 119300.

[14] D. Yu, Y. Qiu, X. Zhang, F. Liu, Research on the energy discharging performance of Y-shaped fin, J. Energy Storage 50 (2022) 104704.

[15] M.S. Mahdi, A.W. Ezzat, H.B. Mahood, Comparative numerical study of melting behavior of a phase change material in shell and tube latent heat energy storage unit with longitudinal, spiral, and annular fins in horizontal and vertical orientations, J. Therm. Sci. Eng. Appl. 15 (081001) (2023).

[16] M.M. Joybari, S. Seddegh, X. Wang, F. Haghighat, Experimental investigation of multiple tube heat transfer enhancement in a vertical cylindrical latent heat thermal energy storage system, Renew. Energy 140 (2019) 234–244.

[17] N. Kousha, M. Rahimi, R. Pakrouh, R. Bahrampoury, Experimental investigation of phase change in a multitube heat exchanger, J. Energy Storage 23 (2019) 292–304.

[18] Vikas, A. Yadav, S. Samir, M. Arı cı, A comprehensive study on melting enhancement by changing tube arrangement in a multi-tube latent heat thermal energy storage system, J. Energy Storage 55 (2022) 105517.

[19] S.H. Park, Y.G. Park, M.Y. Ha, A numerical study on the effect of the number and arrangement of tubes on the melting performance of phase change material in a multi-tube latent thermal energy storage system, J. Energy Storage 32 (2020) 101780.

[20] A. Pourakabar, A.A. Rabienataj Darzi, Enhancement of phase change rate of PCM in cylindrical thermal energy storage, Appl. Therm. Eng. 150 (2019) 132–142.

[21] G.S. Sodhi, K. Vigneshwaran, P. Muthukumar, Experimental investigations of high-temperature shell and multi-tube latent heat storage system, Appl. Therm. Eng. 198 (2021) 117491.

[22] F. Agyenim, The use of enhanced heat transfer phase change materials (PCM) to improve the coefficient of performance (COP) of solar powered LiBr/H2O absorption cooling systems, Renew. Energy 87 (2016) 229–239.

[23] T. Bouhal, S. ed-Dîn Fertahi, T. Kousksou, A. Jamil, CFD thermal energy storage enhancement of PCM filling a cylindrical cavity equipped with submerged heating sources, J. Energy Storage 18 (2018) 360–370.

[24] D.K. Johar, D. Sharma, S.L. Soni, P.K. Gupta, R. Goyal, Experimental investigation on latent heat thermal energy storage system for stationary C.I. engine exhaust, Appl. Therm. Eng. 104 (2016) 64–73.

[25] H. Niyas, C.R.C. Rao, P. Muthukumar, Performance investigation of a lab-scale latent heat storage prototype – Experimental results, Sol. Energy 155 (2017) 971–984.

[26] D. Dandotiya, N.D. Banker, Numerical investigation of heat transfer enhancement in a multitube thermal energy storage heat exchanger using fins, Numer. Heat Transf. Part A: Appl. 72 (5) (2017) 389–400.

[27] Z. Khan, Z.A. Khan, An experimental investigation of discharge/solidification cycle of paraffin in novel shell and tube with longitudinal fins based latent heat storage system, Energy Convers. Manage. 154 (2017) 157–167.

[28] A.H.N. Al-Mudhafar, A.F. Nowakowski, F.C.G.A. Nicolleau, Thermal performance enhancement of energy storage systems via phase change materials utilising an innovative webbed tube heat exchanger, Energy Procedia 151 (2018) 57–61.

[29] R. Anish, V. Mariappan, M. Mastani Joybari, Experimental investigation on the melting and solidification behavior of erythritol in a horizontal shell and multi-finned tube latent heat storage unit, Appl. Therm. Eng. 161 (2019) 114194.

[30] R. Anish, M.M. Joybari, S. Seddegh, V. Mariappan, F. Haghighat, Y. Yuan, Sensitivity analysis of design parameters for erythritol melting in a horizontal shell and multi-finned tube system: Numerical investigation, Renew. Energy 163 (2021) 423–436.

[31] B.G. Abreha, P. Mahanta, G. Trivedi, Thermal performance evaluation of multi-tube cylindrical LHS system, Appl. Therm. Eng. 179 (2020) 115743.

[32] L. Song, S. Wu, C. Yu, W. Gao, Thermal performance analysis and enhancement of the multi-tube latent heat storage (MTLHS) unit, J. Energy Storage 46 (2022) 103812.

[33] Y. Huang, L. Song, S. Wu, X. Liu, Investigation on the thermal performance of a multi-tube finned latent heat thermal storage pool, Appl. Therm. Eng. 200 (2022) 117658.

[34] M. Esapour, M.J. Hosseini, A.A. Ranjbar, Y. Pahamli, R. Bahrampoury, Phase change in multi-tube heat exchangers, Renew. Energy 85 (2016) 1017–1025.

[35] J.M. Mahdi, S. Lohrasbi, D.D. Ganji, E.C. Nsofor, Accelerated melting of PCM in energy storage systems via novel configuration of fins in the triplex-tube heat exchanger, Int. J. Heat Mass Transfer 124 (2018) 663–676.

[36] A.H. Al-Mudhafar, A.F. Nowakowski, F.C. Nicolleau, Performance enhancement of PCM latent heat thermal energy storage system utilizing a modified webbed tube heat exchanger, Energy Rep. 6 (2020) 76–85, Publisher: Elsevier.

[37] H.-O. Sayehvand, S. Abolfathi, B. Keshavarzian, Investigating heat transfer enhancement for PCM melting in a novel multi-tube heat exchanger with external fins, J. Energy Storage 72 (2023) 108702.

[38] A.J. Parry, P.C. Eames, F.B. Agyenim, Modeling of thermal energy storage shell-and-tube heat exchanger, Heat Transf. Eng. 35 (1) (2014) 1–14.

[39] A.K. Raul, P. Bhavsar, S.K. Saha, Experimental study on discharging performance of vertical multitube shell and tube latent heat thermal energy storage, J. Energy Storage 20 (2018) 279–288.

[40] N. Hannoun, V. Alexiades, T.Z. Mai, A reference solution for phase change with convection, Internat. J. Numer. Methods Fluids 48 (11) (2005) 1283–1308, _eprint: https://onlinelibrary.wiley.com/doi/pdf/10.1002/fld.979.

[41] M.A. Dekhil, J.V. Simo Tala, O. Bulliard-Sauret, D. Bougeard, Numerical analysis of the performance enhancement of a latent heat storage shell and tube unit using finned tubes during melting and solidification, Appl. Therm. Eng. 192 (2021) 116866.

[42] M.A. Dekhil, J.V. Simo Tala, O. Bulliard-Sauret, D. Bougeard, Numerical analysis of the effect of the iso-surface fin redistribution on the performance enhancement of a shell-and-tube latent heat thermal energy storage unit for low-temperature applications, J. Energy Storage 56 (2022) 105892.

[43] M. Longeon, A. Soupart, J.-F. Fourmigué, A. Bruch, P. Marty, Experimental and numerical study of annular PCM storage in the presence of natural convection, Appl. Energy 112 (2013) 175–184.